

A microfabricated surface-electrode ion trap for scalable quantum information processing

S. Seidelin,* J. Chiaverini,† R. Reichle, J. J. Bollinger, D. Leibfried, J. Britton, J. H. Wesenberg, R. B. Blakestad, R. J. Epstein, D. B. Hume, J. D. Jost, C. Langer, R. Ozeri, N. Shiga, and D. J. Wineland
NIST, Time and Frequency Division, Boulder, CO

(Dated: February 1, 2008)

We demonstrate confinement of individual atomic ions in a radio-frequency Paul trap with a novel geometry where the electrodes are located in a single plane and the ions confined above this plane. This device is realized with a relatively simple fabrication procedure and has important implications for quantum state manipulation and quantum information processing using large numbers of ions. We confine laser-cooled $^{24}\text{Mg}^+$ ions approximately $40\ \mu\text{m}$ above planar gold electrodes. We measure the ions' motional frequencies and compare them to simulations. From measurements of the escape time of ions from the trap, we also determine a heating rate of approximately five motional quanta per millisecond for a trap frequency of 5.3 MHz.

Recent interest in coherent quantum state control and methods to realize practical quantum information processing (QIP) has led to impressive developments in quantum processing using several different physical systems [1]. Single quantum bit (qubit) rotations, two-qubit gates, and simple quantum algorithms have been implemented. However, perhaps the most significant challenge for any possible physical implementation of a quantum processor is to devise methods that scale to very large numbers of quantum information carriers.

The system of trapped ions is an interesting candidate for QIP because the basic requirements [2] have been demonstrated in separate experiments [1], and several schemes for scaling this system to large numbers of qubits have been proposed [1, 3, 4, 5, 6, 7]. One approach is based on a network of interconnected processing and memory zones where ion qubits are selectively shuttled between zones [3, 6]. Within this approach, miniature linear trap arrays [8, 9, 10, 11] and a three layer T-junction trap [10] have been demonstrated. Since the speed of most multi-ion qubit gates is proportional to the ions' motional frequencies and these frequencies are inversely proportional to the square of the dimensions, we would like to decrease the size of these dimensions. To do this robustly, microfabrication techniques are required. Three-dimensional traps have been demonstrated with boron-doped silicon [12] and monolithically fabricated gallium-arsenide electrodes [11]. A significant simplification in fabrication could be achieved if all trap electrodes reside on a single surface and the ions are trapped above this surface [13]. In this case, the trapping electric fields would be the analog of magnetic fields used in "chip" traps for neutral atoms (see Ref. [14] and references therein). Surface-electrode ion traps have the potential added benefit for scaling that micro-electronics for electrode potential control can be fabricated below the plane of the electrodes [15].

Recently, macroscopic charged particles have been confined in a surface-electrode trap [16]. Storage of atomic ions, however, requires substantially different experimen-

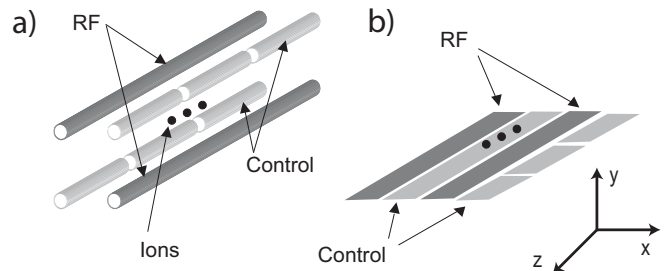


FIG. 1: (a) Standard linear RF Paul trap; (b) Surface-electrode geometry where all electrodes reside in a single plane, with the ions trapped above this plane.

tal parameters. In this letter we report the first demonstration of stable confinement of atomic ions in a surface-electrode trap. The trap is constructed with standard and scalable microfabrication processes. We load $^{24}\text{Mg}^+$ into this trap, measure the motional frequencies of the ions, and find reasonable agreement with those determined from simulations. We also approximately determine a motional heating rate of the ion(s) that is low enough to allow for high fidelity logic operations.

The standard linear radio-frequency (RF) Paul trap [17] consists of four parallel rods whose centers are located on the vertices of a square (Fig. 1a). An RF potential is applied to two opposing rods with the other two (control electrode) rods held at RF ground. This configuration creates a nearly harmonic ponderomotive pseudopotential in the $\hat{x}\text{-}\hat{y}$ plane. Longitudinal confinement for a single trapping zone is obtained by segmenting each control electrode along its length and applying appropriate static potentials to the different segments. Several variations on this design have been demonstrated [8, 9, 10, 11, 12], but it is very desirable to simplify their construction. A straightforward way to modify the 3-D design of Fig. 1a is to place the four rods in a common plane, with alternating RF and control electrodes [13]; one version of this geometry is shown in Fig. 1b. In this design, the rods are replaced with flat

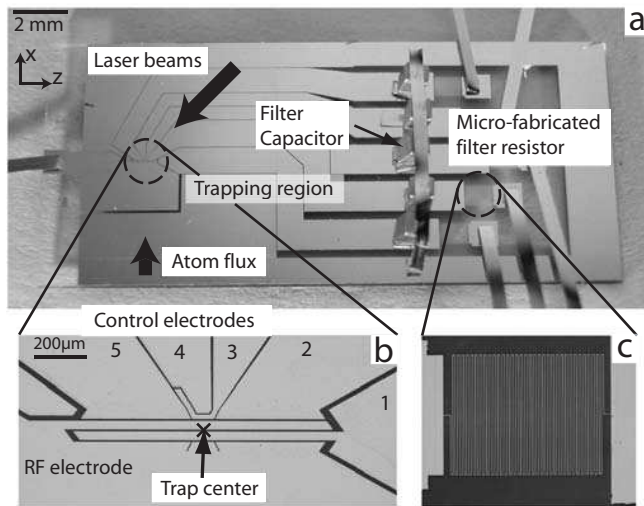


FIG. 2: Pictures of the surface-electrode trap. (a) The complete trap structure, including out-lead wires (ribbons) and filter capacitors. The directions of the laser beams (cooling and photoionization) and atom flux are indicated. (b) Expanded view of the trap region (center marked by \times). The control electrodes are numbered for reference in the text. (c) On-board meander line resistor.

electrodes, as shown in Fig. 2.

We can fabricate this electrode structure by means of photolithography and metal deposition using evaporation and electrodeposition. For the substrate we use polished fused quartz, a material with low RF loss. A $0.030 \mu\text{m}$ titanium adhesion layer and a $0.100 \mu\text{m}$ copper seed layer are first evaporatively deposited onto the substrate. This deposition is uniform except for small areas for resistors where the quartz is left exposed. Resistors ($\sim 1 \text{ k}\Omega$) and leads are fabricated through a liftoff process that entails patterning them with standard photolithography and evaporation of a $0.013 \mu\text{m}$ titanium adhesion layer followed by $0.300 \mu\text{m}$ of gold. Resistors are fabricated directly on the quartz substrate; leads are fabricated on top of the copper seed layer. The gold electrodes near the trapping region are electroplated onto the copper seed layer after a second photolithographic patterning step. Afterward, the exposed initial seed and adhesion layers are etched away to isolate electrodes and leads. The trap electrodes are plated to a thickness of $\sim 6 \mu\text{m}$ so that the ratio of height to inter-electrode spacing is relatively high (the inter-electrode spacing is $\sim 8 \mu\text{m}$). This should reduce alteration of the trapping potential due to stray charges that may collect on the exposed insulator between electrodes.

We create ions in the trap by photoionizing thermally evaporated neutral magnesium atoms. The magnesium source is realized by resistively heating a stainless steel tube containing solid magnesium, which is sealed at both ends and has a small slit from which evaporated magnesium atoms emerge. With a planar electrode geometry,

there is a risk of shorting electrodes to each other due to magnesium deposited onto the trap structure. To reduce this risk, in a last processing step we perform a controlled hydrofluoric acid (HF) etch of the central trap region. The HF etches away a small part of the titanium adhesion layer and the substrate, without affecting the electrodes. The result is a $\sim 2 \mu\text{m}$ horizontal undercut of the electrodes to help prevent shorting due to deposition from the magnesium source. As a further precaution, we direct the magnesium flux nearly parallel to the surface and avoid as much as possible having the channels between electrodes be parallel to the flux (Fig. 2).

We use five independent control electrodes to provide sufficient degrees of freedom to be able to overlap the electric field null point of the static potential and the RF pseudopotential minimum. We create a low impedance path for the RF to ground on the control electrodes with capacitors (820 pF) that are surface mounted directly onto the chip (in the future, capacitors could be included as part of the fabrication process). Gold ribbons for applying the electrode potentials are gap-welded to contact pads.

The trap structure is mounted in a copper tube that also serves as part of an RF transformer [18] and the entire structure is surrounded by a quartz envelope. The system is baked under vacuum prior to operation to reach a base pressure below 10^{-8} Pa with the use of an ion getter pump combined with a titanium sublimation pump.

As we describe below, the trap well depth U_T for a surface-electrode trap is fairly shallow [13], not much above the mean kinetic energy of the neutral atoms before they are ionized. Nevertheless, we can load $^{24}\text{Mg}^+$ ions efficiently by resonant two-photon photoionization (PI) at 285 nm [19]. The PI laser, resonant with the $3s^2 \ ^1S_0 \leftrightarrow 3s3p \ ^1P_1$ electric dipole transition in neutral magnesium, co-propagates with a Doppler cooling beam tuned approximately 400 MHz below the $3s \ ^2S_{1/2} \leftrightarrow 3p \ ^2P_{1/2}$ electric dipole transition in $^{24}\text{Mg}^+$ at 280 nm . The laser beams are parallel to the trap surface, and at an angle of approximately 45 degrees with respect to the trap \hat{z} axis as shown in Fig. 2a.

Since the laser beam direction has significant overlap with all principal trap axes, cooling will be efficient in all directions [13]. During loading, both the Doppler cooling and PI beams have 2 mW power and waists of $\sim 40 \mu\text{m}$. The atomic flux of magnesium intersects the laser beams at the trap (Fig. 2a). The cooling beam is applied continuously, while the PI beam needs to be applied for only a few seconds to create ions in the trap. Ions are detected by observing $3p \ ^2P_{1/2} \rightarrow 3s \ ^2S_{1/2}$ fluorescence along a direction perpendicular to the trap surface with a CCD camera as in the view of Fig. 2b. Despite the fact that the center of the laser beam is only $40 \mu\text{m}$ above the surface, which increases the risk of scatter from light striking the trap electrodes, the signal-to-background ratio for scattered light from the ions is greater than 100

when the Doppler cooling laser is tuned approximately 20 MHz (one-half linewidth) below resonance with intensity slightly below saturation.

We measure the oscillation frequencies for a single ion in the trap (equal to the center-of-mass mode frequencies for multiple ions) by applying an oscillating field to a control electrode and observing a change in fluorescence rate when the frequency of the applied field is equal to one of the motional frequencies, thereby heating the ion [18]. To excite the axial mode, we apply the oscillating field to electrode 2, while both transverse modes can be excited using electrode 1.

As an aid in initially determining the correct operating conditions, trapping potentials are determined using numerical solvers (boundary element method) subject to the constraint that the RF pseudopotential minimum overlaps the null points of the electric field from the static potential, to minimize RF micromotion (see for example [20]). For the experiments described here, the static potentials on each control electrode, expressed as a fraction of the potential V_5 on electrode 5 (Fig. 2b) are $V_1 = 0.320$, $V_2 = 0.718$, $V_3 = 0.738$, and $V_4 = -0.898$.

The peak potential amplitude V_{RF} applied to the RF electrode (at a frequency of 87 MHz) is difficult to measure directly. To determine it, we measure the three mode frequencies for a fixed RF power and $V_5 = 5.00$ V. We use the simulations with the measured electrode dimensions to extract a best fit value of $V_{\text{RF}} = 103.5$ V. The consistency between the experimental and simulated frequencies for this fit is shown in Table I. We further check for consistency by comparing the measured and predicted mode frequencies for two other values of the control and RF potentials (also shown in Table I). The value $V_{\text{RF}} = 46.2$ V is determined by scaling the RF power delivered to the trap. The agreement between predicted and measured frequencies is within a few percent. Finally, we determine numerically the overall potential depth U_T in the pseudopotential approximation [21, 22] for the different control and RF potentials (also shown

TABLE I: Oscillation frequencies (experimental measurements (Exp.) and simulated values (Sim.)) for three different potential configurations explained in the text. The axial frequency is denoted f_{\parallel} , while $f_{\perp 1}$ and $f_{\perp 2}$ are the frequencies of the two transverse modes whose axes are indicated by the cross in Fig. 3. The uncertainties in the experimental values for the frequencies are approximately 0.10 MHz.

| V_5 (V) | V_{RF} (V) | f_{\parallel} (MHz) | $f_{\perp 1}$ (MHz) | $f_{\perp 2}$ (MHz) | U_T (meV) | |
|--------------|------------------------|--------------------------|------------------------|------------------------|----------------|--------|
| 5.00 | 103.5 | 2.83 | 15.78 | 17.13 | | (Exp.) |
| | | 2.77 | 15.67 | 17.21 | 177 ± 6 | (Sim.) |
| 2.00 | 103.5 | 1.84 | 15.87 | 16.93 | | (Exp.) |
| | | 1.75 | 16.23 | 16.87 | 193 ± 11 | (Sim.) |
| 5.00 | 46.2 | 2.85 | 5.28 | 8.29 | | (Exp.) |
| | | 2.77 | 5.05 | 8.75 | 6 ± 1 | (Sim.) |

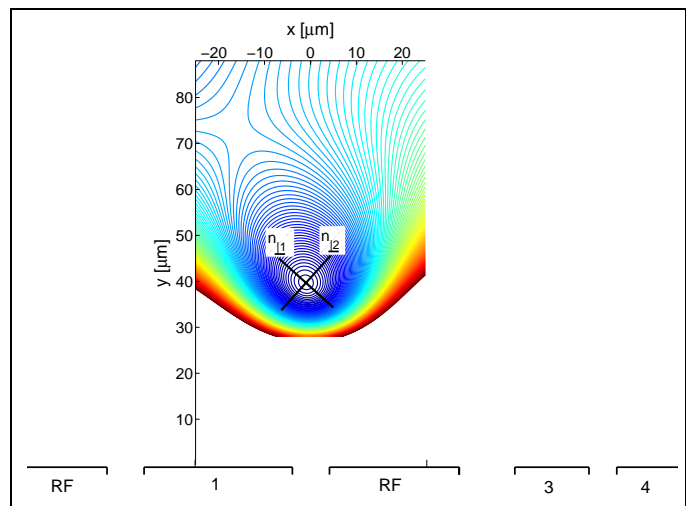


FIG. 3: A transverse cross-section of the simulated trapping potential (both RF pseudopotential and static potentials included) for potentials corresponding to $V_5 = 5.00$ V and $V_{\text{RF}} = 103.5$ V ($U_T = 177$ meV). The cross indicates the directions of the normal mode axes $\mathbf{n}_{\perp 1}$ and $\mathbf{n}_{\perp 2}$, and the expected position for an ion at the center of the trap in the \hat{x} - \hat{y} plane. The separation between contour lines corresponds to 5 meV and the colors blue to red correspond to low to high potential. The electrodes are depicted to scale in the lower part of the figure and labeled as in Fig. 2b.

in Table I). A transverse cross-section (the \hat{x} - \hat{y} plane of Fig. 1b) of the trapping potential for $V_5 = 5$ V and $V_{\text{RF}} = 103.5$ V near the central trap region is shown in Fig. 3.

In Fig. 4, we show groups of ions for the $V_{\text{RF}} = 103.5$ V and $V_5 = 2.00$ V configuration. The separation of the ions is related to the center-of-mass axial oscillation frequency [3], and the horizontal bars indicate the expected ion separations according to the measurement of this frequency (1.84 ± 0.10 MHz for this configuration). When the number of ions becomes large enough, the string breaks into a zig-zag configuration (see for example [23]).

Because $^{24}\text{Mg}^+$ lacks hyperfine structure, we cannot easily determine heating rates near the quantum limit (without applying large magnetic fields) due to poor internal state discrimination [24]. However, an approximate value of the transverse mode heating rate can be determined by observing how long an ion remains trapped in a shallow well in the absence of the Doppler cooling light [11]. If we assume the heating rate (the energy change per unit of time) is constant until the ion can overcome the saddle-point in Fig. 3, we can estimate the initial heating rate as $\langle r \rangle \simeq U_T / (\langle \tau_s \rangle h f_{\perp 1})$ quanta per second, where $\langle \tau_s \rangle$ is the average survival time of the ion in absence of cooling light, h is Planck's constant and $f_{\perp 1}$ is the smaller of the two transverse mode frequencies.

To help ensure that the results are not influenced by the ions thermalizing to the ambient temperature (~ 300

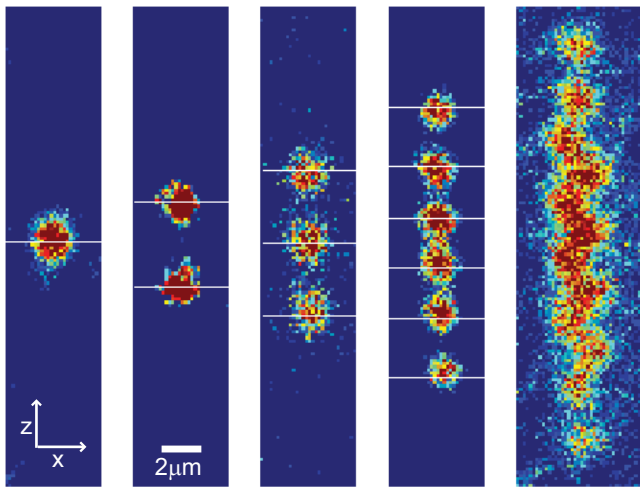


FIG. 4: False-color images of one, two, three, six, and 12 ions loaded into the surface trap (red corresponds to highest fluorescence count rate). The length scale is determined from a separate image of the electrodes whose dimensions are known. The horizontal bars indicate the separation distance between the ions as predicted from the measured axial oscillation frequency. The ratio between transverse and axial oscillation frequencies makes it energetically favorable for the 12 ion string to break into a zig-zag shape (see for example [23]).

$K \simeq 25$ meV) we perform the measurements of $\langle \tau_s \rangle$ with a very shallow well depth, $U_T = 6 \pm 1$ meV ($V_5 = 5$ V, $V_{RF} = 46.2$ V, and $f_{\perp 1} \simeq 5.3$ MHz). From these data, we determine $\langle \tau_s \rangle = 53 \pm 10$ s, and find $\langle r \rangle \simeq 5$ quanta per millisecond.

Johnson noise in the resistance of the RC filters on the control electrodes is a potential source of heating [3], but we theoretically estimate it to contribute only 1 quantum per second. Therefore the observed heating is apparently dominated by anomalous heating as observed in previous experiments [25]. We note that in presence of Doppler cooling light, the lifetime of the ion is several hours (in the trap with $U_T = 177$ meV), presumably limited by chemical reactions [26].

Heating and decoherence rates for small ion traps will be an important issue for future implementations of quantum information processing, and will need to be more thoroughly investigated. Therefore, an important next step is to replace the $^{24}\text{Mg}^+$ with an isotope that allows for Raman sideband cooling, such as $^{25}\text{Mg}^+$ or $^9\text{Be}^+$, and to study heating rates near the ground state of motion [24, 25]. A longer-term goal is to design and fabricate a surface trap with more complex structures involving T- or X-junctions with separate memory- and processing zones.

We thank E. Langlois and J. Moreland for advice on the micro-fabrication processes and Y. Le Coq for helpful comments on the manuscript. This work was supported by the Advanced Research and Development Activity (ARDA) under contract MOD-7171.05 and NIST.

S. S. wishes to thank the Carlsberg Foundation for financial support. This manuscript is a publication of NIST and not subject to U. S. copyright.

* Electronic address: seidelin@boulder.nist.gov

† Present Address: Los Alamos National Laboratory

- [1] See for instance http://qist.lanl.gov/qcomp_map.shtml.
- [2] DiVincenzo, Fortschr. Phys. **48**, 771 (2000).
- [3] D.J. Wineland, C. Monroe, W.M. Itano, D. Leibfried, B.E. King, and D.M. Meekhof, J. Res. Nat. Inst. Stand. Tech. **103**, 259 (1998).
- [4] R.G. DeVoe, Phys. Rev. A **58**, 910 (1998).
- [5] J.I. Cirac and P. Zoller, Nature **404**, 579 (2000).
- [6] D. Kielpinski, C. Monroe and D.J. Wineland, Nature **417**, 709 (2002).
- [7] L.-M. Duan, B.B. Blinov, D.L. Moehring, and C. Monroe, Quant. Inform. Comp. **4**, 165 (2004).
- [8] M.A. Rowe, A. Ben-Kish, B. DeMarco, D. Leibfried, V. Meyer, J. Beall, J. Britton, J. Hughes, W.M. Itano, B. Jenkovic, C. Langer, T. Rosenband, and D.J. Wineland, Quant. Inform. Comp. **2**, 257 (2002).
- [9] M.D. Barrett, J. Chiaverini, T. Schaetz, J. Britton, W.M. Itano, J.D. Jost, E. Knill, C. Langer, D. Leibfried, R. Ozeri, D.J. Wineland, Nature **429**, 737 (2004).
- [10] W.K. Hensinger, S. Olmschenk, D. Stick, D. Hucul, M. Yeo, M. Acton, L. Deslauriers, J. Rabchuk, C. Monroe, quant-ph/0508097.
- [11] D. Stick, W.K. Hensinger, S. Olmschenk, M.J. Madsen, K. Schwab and C. Monroe, Nature Physics **2**, 36 (2006).
- [12] D.J. Wineland, D. Leibfried, M.D. Barrett, A. Ben-Kish, J.C. Bergquist, R.B. Blakestad, J.J. Bollinger, J. Britton, J. Chiaverini, B. DeMarco, D. Hume, W.M. Itano, M. Jensen, J.D. Jost, E. Knill, J. Koelemeij, C. Langer, W. Oskay, R. Ozeri, R. Reichle, T. Rosenband, T. Schaetz, P.O. Schmidt, S. Seidelin, in Proc. XVII Int. Conf. on Laser Spectroscopy, Avemore, Scotland, 2005, ed. by E. A. Hinds, A. Ferguson, and E. Riis (World Scientific, Singapore, 2005), pp. 393-402 (quant-ph/0508025).
- [13] J. Chiaverini, R.B. Blakestad, J. Britton, J.D. Jost, C. Langer, D. Leibfried, R. Ozeri and D.J. Wineland, Quant. Inform. Comp. **5**, 419 (2005).
- [14] R. Folman, P. Krüger, J. Schmiedmayer, J. Denschlag and C. Henkel, Adv. Atom. Mol. Phys. **48**, 263 (2002).
- [15] J. Kim, S. Pau, Z. Ma, H.R. McLellan, J.V. Gages, A. Kornblit, and R.E. Slusher, Quant. Inform. Comp. **5**, 515 (2005).
- [16] C.E. Pearson, D.R. Leibbrandt, W.S. Bakr, W. J. Mallard, K. R. Brown, and I. L. Chuang, quant-ph/0511018.
- [17] W. Paul, Rev. Mod. Phys. **62**, 531 (1990).
- [18] S.R. Jefferts, C. Monroe, E.W. Bell, and D.J. Wineland, Phys. Rev. A **51**, 3112 (1995).
- [19] D.N. Madsen, S. Balslev, M. Drewsen, N. Kjærgaard, Z. Videsen and J.W. Thomsen, J. Phys. B: At. Mol. Opt. Phys. **33**, 4981 (2000).
- [20] D.J. Berkeland, J.D. Miller, J.C. Bergquist, W.M. Itano, and D.J. Wineland, J. Appl. Phys. **83**, 5025 (1998).
- [21] H.G. Dehmelt, Adv. Atom. Mol. Phys. **3**, 53 (1967).
- [22] P.K. Ghosh, *Ion Traps* (Clarendon Press, Oxford, 1995).
- [23] Daniel H.E. Dubin, Phys. Rev. Lett. **71**, 2753 (1993).
- [24] C. Monroe, D.M. Meekhof, B.E. King, S.R. Jefferts,

- W.M. Itano, D.J. Wineland and P. Gould, Phys. Rev. Lett. **75**, 4011 (1995).
- [25] Q.A. Turchette, Kielpinski, B.E. King, D. Leibfried, D.M. Meekhof, C.J. Myatt, M.A. Rowe, C.A. Sackett, C.S. Wood, W.M. Itano, C. Monroe, and D.J. Wineland, Phys. Rev. A. **61**, 063418 (2000).
- [26] K. Mølhave and M. Drewsen, Phys. Rev. A. **62**, 011401 (2002).